Title: An optogenetic tool to raise intracellular pH in single cells and drive localized membrane dynamics

Author List: Caitlin E. T. Donahue[1,2], Michael D. Siroky[1,2], and Katharine A. White[1,2]

Institution Address: [1]Department of Chemistry and Biochemistry, University of Notre Dame, Notre Dame, IN, USA and [2]Harper Cancer Research Institute, University of Notre Dame, Notre Dame, IN, USA

Corresponding author: Katharine A. White – Department of Chemistry and Biochemistry and Harper Cancer Research Institute, University of Notre Dame, Notre Dame, IN, USA
Email: kwhite6@nd.edu

Abstract:

Intracellular pH (pHi) dynamics are critical for regulating normal cell physiology. For example, transient increases in pHi (7.2-7.6) regulate cell behaviors like cell polarization, actin cytoskeleton remodeling, and cell migration. Most studies on pH-dependent cell behaviors have been performed at the population level and use non-specific methods to manipulate pHi. The lack of tools to specifically manipulate pHi at the single-cell level has hindered investigation of the role of pHi dynamics in driving single cell behaviors. In this work, we show that Archaerhodopsin (ArchT), a light-driven outward proton pump, can be used to elicit robust and physiological pHi increases over the minutes timescale. We show that activation of ArchT is repeatable, enabling the maintenance of high pHi in single cells for approximately 45 minutes. We apply this spatiotemporal pHi manipulation tool to determine whether increased pHi is a sufficient driver of membrane ruffling in single cells. Using the ArchT tool, we show that increased pHi in single cells can drive localized membrane ruffling responses within seconds and

increased membrane dynamics (both protrusion and retraction events) compared to control cells. Overall, this tool allows us to directly investigate the relationship between increased pHi and cell behaviors such as membrane ruffling. This tool will be transformative in facilitating the experiments required to determine if increased pHi is a driver of these cell behaviors at the single-cell level.

INTRODUCTION

In normal epithelial cells, intracellular pH (pHi) is regulated between 7.0-7.2, but transient increases in pHi (7.2-7.6) are linked to cell behaviors including cell polarization[1,2], cytoskeleton remodeling[3,4], and directed cell migration.[1,2,5,6] However, most studies on pH-dependent cellular behaviors pHi using non-specific methods[7], which can confound interpretation of biological cause and effect. The lack of appropriate tools to specifically and spatiotemporally manipulate pHi in living cells has obscured our understanding of pHi-dependent regulation of cell behaviors and severely limited identification of the molecular mechanisms underlying pH-dependent behaviors. Elucidating these molecular mechanisms will advance our understanding of the normal mechanism of these behaviors and ultimately enable us to identify where these are dysregulated in disease states such as cancer (constitutively increased pHi) and neurodegenerative diseases (constitutively decreased pHi).

Current methods to manipulate intracellular pHi are nonspecific and technically challenging.[7] For example, genetic overexpression[8] or ablation[9] of ion transporters alter pHi but lack specificity, as ion transporters can be linked to non-proton gradient changes[10] and function as signaling scaffolds.[11] Furthermore, the use of ion transport inhibitors is very common[12,13] but recent studies have reported significant off-target effects of various pHi-lowering drugs.[14,15]

Micropipette pHi manipulation techniques are highly specific and adaptable to single-cell analysis.[16] However, micropipette pHi manipulation is technically challenging, has poor temporal control, is damaging to the cell, and is low-throughput.[17] Proton uncaging molecules can be photolysed to release protons with good temporal control. However, spatial control of proton uncaging is poor, requires UV photolysis which is cytotoxic, and proton uncaging can only be used to lower pHi, limiting experimental applications.[18–21] The ideal tool to spatiotemporally manipulate pHi in single cells would be non-damaging to the cell, have good spatial and temporal control, be robust and reversible, and allow for repeated pHi manipulations.

We identified Archaerhodopsin (ArchT), an outward proton pump activated by 561 nm light, as a potential tool to spatiotemporally raise pHi in single cells. Archaerhodopin is natively light-activatable, expressed on the plasma membrane, and is a viable first generation pHi manipulation tool. Archaerhodopsins have been previously developed as light-activated neuronal silencers.[22,23] Under long (15sec) photoactivation conditions, ArchT did not significantly increase pHi in neurons.[23] However, recent work suggests that ArchT could be a viable tool for pHi manipulation. First, a study used an adapted ArchT with ER export for improved surface expression to increase pHi locally in the spatially-restricted synaptic bouton under very long (2 minute) photoactivation conditions.[24] Second, ArchT was recently used as a high-resolution spatiotemporal tool to generate proton fluxes to measure gap junction connectivity in mammalian cells and the developing *Drosophila* brain.[25] Based on these foundational studies, we hypothesized that ArchT could be adapted to reversibly and robustly manipulate intracellular pHi in mammalian cells on the minutes timescale.

In this work, we show the optimization and characterization of ArchT to spatiotemporally raise pHi in single cells. Using optimized photoactivation protocols, we can robustly raise pHi in

single cells over the minute-timescale. The ArchT-induced pHi response can be seen with a range of light power used, and we can induce a range of physiological increases in pHi (0.10-0.4), similar to those reported during pH-regulated processes (0.1-0.35). Furthermore, we show that this tool can be repeatedly photoactivated, allowing for sustained pHi manipulation on a longer timescale (~45 minutes). When we raise pHi spatiotemporally using ArchT in single living cells, we found that increased pHi drives localized membrane ruffling responses in single cells. ArchT is a robust optogenetic tool for spatiotemporally increasing cytosolic pH within single-cells.

METHODS

Cell Culture NIH-3T3 mouse embryo fibroblast (NIH-3T3 ATCC® CRL-1658) cells were cultured in Dulbecco's Modified Eagle's Medium (DMEM, Corning 10-013-CV) supplemented with 10% Fetal Bovine Serum (FBS, Peak Serum, PS-FB2). Retinal Pigment Epithelial (RPE, ATCC® CRL-4000) cells were cultured in Roswell Park Memorial Institute 1640 media (RPMI-1640, Corning, 10-040-CV), supplemented with 10% FBS (Peak Serum, PS-FB2) and GlutaMAX™ (Gibco, 35050-061) up to 446 mg/L of glutamine. All cells were grown in humidified incubators at 37°C, 5% CO_2.

Plasmid Constructs pcDNA3.1-ArchT-BFP2-TSERex was a gift from Yulong Li (Addgene plasmid # 123312) pCDNA3-mCherry-SEpHluorin (mCherry-pHluorin) was a gift from Sergio Grinstein (Addgene plasmid #32001)

Transfection Protocol RPE and NIH-3T3 cells were transiently transfected using Lipofectamine 2000 (Life Technologies, 11668-019) Briefly, a 1:1 ratio of DNA-Lipofectamine complex was

prepared in 1 mL serum-free media (DNA: 2 µg of a single-construct or 1µg of each construct for double transfection) (Lipofectamine: used at 3:1 ratio to DNA). This was then added to 1 mL serum-free media on cells. Cells were incubated with transfection media for 8 hours at 37°C with 5% CO_2, before exchanging with complete media. Cells were imaged the following day.

Microscopy All imaging experiments were performed using a Nikon Ti2 Eclipse confocal microscope equipped with a spinning disk (CSU-X1, Yokogawa) using solid-state lasers (395 nm, 488 nm, 561 nm) with appropriate filter sets (BFP: ET455/50M, GFP: ET525/36M, mCherry: ET605/52M) on 60x objectives (CFI PLAN APO OIL, NA=1.40, NIKON), using a CMOS camera (ORCA-Flash4.0). Cells were imaged in 35 mm imaging dishes (Matsunami, Dd35-14-1.5-U) within a stage-top environmental chamber (Tokai) at 37°C and 5% CO_2. Photoactivation experiments used a digital micromirror device patterned illumination system (Polygon 4000, Photometrix). All microscope control and image analysis used Nikon NIS Elements AR software.

Photoactivation Protocol A small section of the cell was identified and illuminated using a user-defined region of interest (ROI) within Nikon NIS Elements AR Illumination Sequence Module. In all experiments, the Polygon400 and illumination/stimulation sequences were directly triggered by the camera. The standard illumination/stimulation sequence: 3 seconds of pHluorin (488 ex/525 em) pulsed acquisition (25 msec exposure every 50 msec) followed by 3 seconds of continuous 561 nm LED illumination to activate ArchT (power between 1% and 100%, see figure legends for details) with pHluorin (488 ex/525 em) pulsed co-acquisition (25 msec exposure every 50 msec). This pattern was repeated for a total of 154 seconds. For membrane dynamics experiments, an additional 30 sec of pHluorin (488 ex/525 em) pulsed

acquisition was added both before and after the standard 154 sec pulsed protocol, for a total acquisition time of 215 sec.

LED titration and stimulation repeatability experiments (Figure 2, S3) The LED power optimization and ArchT repeatability experiments were automated using the JOBs module within NIS Elements AR. For the power titration curves, the 154s illumination sequence (as described above) was looped with a rest period (no acquisition or illumination) of 2 minutes before the pattern repeated for the next LED power. For decreased power titration 100%, 50%, 20%, 10%, 1% LED power sequence was used. For increased power titration 10%, 20%, 30%, 50%, 100% sequence was used. For the repeatability assays, the illumination sequence pattern at 100% LED power was looped with a rest for 2 minutes. This illumination sequence pattern was performed 10 times on each cell.

pHi Calculation We were not able to directly calculate pHi from pHluorin/mCherry ratios as previously described[8] because mCherry visualization activates ArchT within the cells. Instead, we collected representative datasets of pHi measurements as previously described[8] in both RPE and NIH-3T3 cells transfected with mCherry-pHluorin but not ArchT. Briefly, pHluorin/mCherry ratios were obtained for individual cells under standard culture conditions. Then pH standard buffers (pH ~6.5 and ~7.5 (0.025 M HEPES, 0.105 M KCl, 0.001 $MgCl_2$)) were prepared with 10 μM nigericin (Invitrogen, N1495) (a protonophore) and added to cells to equilibrate pHe and pHi as previously described.[26] For each cell, a standard curve was calculated using pHluorin/mCherry ratios at the high and low pHi standards. Using the standard curve data from pHi measurements in RPE and NIH-3T3 cells, we calculated the average intensity change in pHluorin per pH unit. For Figure 1, 2, S1, S2, S3, and S4, the intensity change of each cell at 30 sec and 154 sec was converted to give change in pHi.

Data Analysis Images were processed using Nikon Elements AR software. Images were background subtracted using an ROI placed on an area without visible cells within the field of view (Figures 1, 2, S1, S2, S3, and S4). ROIs were drawn on each cell using the pHluorin fluorescence signal and average ROI intensity values were obtained for pHluorin (pH-sensitive fluorescence) and mCherry (expression normalizer, where indicated in methods).

Photobleaching correction (Figures 1, 2, S1, S2, S3, and S4). Briefly, average pHluorin ROI intensities of control cells were normalized to t = 0 and an average photobleaching curve was calculated from these individual curves. Data were corrected, with ArchT stimulated and non-stimulated cells corrected with matched control photobleaching curves.

Localized membrane protrusion (Figures 4, 5, and S5). A Nikon Elements AR General Analysis 3 (GA3) analysis pipeline was developed with the help of Nikon Instruments Inc. Software Support (Yu-Chen Hwang Ph.D., Biosystems Technical Solutions Manager). Briefly, each cell was segmented into 2 μm concentric segments originating from the circular stimulation ROI. For each concentric circle, total cell area and mean pHluorin intensity were determined within the segmented region. Change in area was tracked over time as a readout of local membrane protrusion events.

Statistical Analysis Normality of all of data was tested using Shapiro-Wilk normality test. For normally-distributed data (Figure 2), statistical significance was determined using a one-way ANOVA with Tukey multiple-comparisons correction. For non-normally distributed data (Figure 1, S1, S2, S4), statistical significance was determined using the Kruskal-Wallis test with Dunn's multiple-comparisons correction. Significance for the LED power titration experiments (Figure S3) were determined using two-way ANOVA and Holm-Šídák's multiple comparison test, and sphericity was assumed for these analyses.

RESULTS AND DISCUSSION

ArchT induces spatiotemporal increases in pHi at the single-cell level

In our first validation experiment, we tested whether we could achieve spatiotemporal pHi increases in single human retinal epithelial (RPE) cells expressing ArchT (Figure 1A). We observed good membrane localization of ArchT fused to blue fluorescent protein (BFP2) with an ER export signal (ArchT-BFP2-TSERex)[25] (Figure S1A), and co-transfected a genetically encoded pH biosensor (mCherry-pHluorin)[27] to monitor pHi changes in real time. Using a digital micromirror device (DMD), we can spatially restrict 561 nm photoactivation of ArchT to just a single cell (Figure 1A). If our tool and microscopy setup enable spatiotemporal pHi manipulation, we would expect to observe increased pHi (increased pHluorin intensity) only in the stimulated cell (Figure 1A).

We photoactivated a single ArchT-expressing cell with 561 nm light using a 2.5 minute photomanipulation protocol (see methods). We observed a robust increase in pHluorin intensity in the light-stimulated cell, while there was no net change in pHluorin intensity in control cells (no ArchT) and ArchT expressing unstimulated cells within the same field of view over the course of the experiment (Figure 1B, C). This result was confirmed across many ArchT cells, where we observed a rapid increase in pHluorin intensity within just 30 seconds that plateaus by the end of the assay (Figure 1D). Non-stimulated ArchT cells did not exhibit a significant increase in pHluorin fluorescence, indicating spatially restricted photoactivation (Figure 1D-E, Figure S1B (30 sec)). Importantly, pHluorin signal did not increase in control cells, regardless of whether they were stimulated with light (Figure 1D-E and Figure 1SB (30 sec)). Thus, the pHluorin response requires both expression of the ArchT tool and light activation.

We were able to quantify pHi increases induced by ArchT in single cells (see methods). We found that ArchT stimulated cells increased pHi by an average of 0.14 ± 0.03 (mean ± SEM) pH units after 30 seconds (Figure 1SC) and 0.18 ± 0.04 (mean ± SEM) pH units by the end of the experiment, 154 seconds (Figure 1F). At the end of the stimulation period, ArchT expressing cells that were stimulated were the only cells in which a significant increase in pHi was observed compared to zero ($p<0.0001$). Importantly, these pHi increases correspond well with physiological pHi increases (0.1-0.35) observed during normal cell behaviors like directed cell migration[1,2,5,26], cell polarization[1,2], and cell cycle progression[28].

ArchT induces robust pHi increases at low and high stimulation powers

We next sought to determine the range of LED stimulation powers that can be used to induce a robust pHi increase. We note that when using the strongest LED power (100%) in RPEs we would expect both heat effects and potential for ArchT dark activation to be high. When using 100% LED power in RPEs (Figure S2) we saw a similar pHi increase for ArchT cells (0.10 ± 0.04), at the end of the experiment, compared to the lower 30% laser power experiments (Figure 1). At 100% stimulation power, we did observe increased ArchT dark-activation, leading to both stimulated and non-stimulated ArchT cells demonstrating an increase in pHi (compared to zero, $p<0.05$) at the end of the experiment. This likely reflects increased light-bleedthrough outside the stimulation ROI at 100% LED power, leading to increased measured "dark activation" of ArchT. However, we saw no increase in pHi in stimulated control cells, indicating heat effects alone are not sufficient to induce pHi changes observed in these assays. These data suggests that even the highest LED stimulation settings produce robust and specific increases in pHi in ArchT stimulated cells compared to control cells (Figure S2).

It would be advantageous if ArchT could be specifically activated to raise pHi using a range of LED stimulation powers to be adaptable to various experimental applications. To test this, we first titrated LED power sequentially up from 10% to 100% LED power and observed statistically significant increases in pHi compared to control at as little as 10% power (Figure S3A, B). We also titrated LED power sequentially down from high intensity (100%) to low intensity (1%) to control for potential prolonged heat effects producing a different outcome on control cell responses. In this case, we found that pHi was increased compared to control as low as 20% LED power (Figure S3C, D). At the end of stimulation period, we observe no significant differences in pHi increases achieved with LED stimulation ranging from 1% to 100%. We also observe significant increases in pHi (compared to zero, $p<0.0001$) within ArchT stimulated cells for stimulation powers as low as 10% whether titrating up or down in power. This shows that the ArchT tool can be stimulated using a wide-range of LED powers to fit the imaging needs of the user. In particular, these results show that lower LED stimulation powers can be used to significantly raise pHi if phototoxicity, photobleaching, or heat-effects are a concern in sensitive applications. Collectively, this data demonstrates that ArchT can be used to elicit robust pHi responses under various LED stimulation conditions.

ArchT-induced pHi increases are repeatable within single cells

We have shown that the ArchT tool can be used to increase pHi in single-cells in real time and we observe efficient and robust increases in pHi using a range of LED stimulation powers. Next, we determined whether the ArchT tool can be used to repeatedly and reversibly increase pHi in a single cell. Achieving repeatable pHi manipulations will enable investigation of pH-dependent cell behaviors that occur on longer timescales, such as cell polarization and

migration. As a proof of principle, we stimulated an RPE cell expressing ArchT and the pH biosensor with 561 nm light using the optimized 2.5-minute stimulation protocol (see methods), and then we allowed the cell to recover for 2 minutes. This pattern was repeated for a total of 10 stimulations on the same individual targeted cell (Figure 2A). As expected, within each stimulation period we observed a rapid increase in pHluorin intensity in the light-stimulated ArchT cell, followed by a plateauing of the response, while the control cells were non-responsive (Figure 2B). However, between stimulation periods, pHluorin intensity recovered to baseline levels, suggesting that the cells were returning to pHi homeostasis during the rest period (Figure 2B). This result was robust across many ArchT and control cells over the 45-minute repeated stimulation protocol (Figure 2C). Notably, the measured increase in pHi in ArchT cells during stimulation windows was consistent and robust (Figure 2D). This data suggests that the ArchT tool can be used to repeatedly and reliably raise pHi in cells over a 45-minute protocol. Furthermore, these results suggest that ArchT may be an appropriate tool to investigate pH-dependent cell behaviors, such as cell polarization, that occur on a longer timescale.[29]

Increases in pHi are sufficient to drive membrane ruffling

We next applied ArchT to investigate the relationship between spatiotemporally increased pHi and single-cell membrane ruffling responses, which occur on the order of seconds to minutes[3,4,30]. The ArchT tool enables us to determine whether localized pHi increases produce global or localized membrane ruffling responses in single cells (Figure 3A). One hypothesis is that protons are diffusible and thus a local pHi increase would quickly produce a global (non-localized) membrane ruffling response.[31] An alternative hypothesis is that localized increases in pHi could be maintained or reinforced by protein recruitment[32] to produce localized membrane

ruffling responses. With ArchT as a tool for spatiotemporal pHi manipulation, we can now determine if increased pHi is sufficient or necessary for membrane remodeling in single-cells. We selected mouse fibroblasts NIH-3T3 (NIH-3T3) cells because they form more pronounced lamella than RPE cells, making them ideal for investigating the relationship between increased pHi and membrane ruffling. We first validated that ArchT could produce similar pHi increases in NIH-3T3 cells (Figure S4) and observed comparable specificity and pHi changes to those we observed in RPE cells. At the end of the stimulation period, we observe significant increases (compared to 0) in ArchT stimulated cells ($p<0.01$), but not in ArchT non-stimulated cells or control cells. This suggests that ArchT can be used to produce robust physiological and spatiotemporal increases in pHi in single NIH-3T3 cells.

We expressed ArchT in NIH-3T3 cells and stimulated the thin-lamella portions of the cell with 561 nm light. We observed that the thin-lamella region within and around the stimulation ROI underwent a distinct and localized membrane ruffling response in ArchT cells that was not observed in control cells (Figure 3B, Supplementary Videos 1 (ArchT) and 2 (Control)). In order to better analyze this response, we traced the outline of the stimulated cell at various time points throughout the experiment. From these traces, we can see that the ArchT cell is much more dynamic in the stimulation region compared to the control cell (Figure 3C). The ArchT cell starts with a pronounced lamella protrusion at the top-left of the cell (Figure 3C, red trace) and ends with the protrusion extended above and to the bottom right of the stimulation ROI (Figure 3C, purple trace). Additional examples of ArchT and control cell traces can be found in Figure S5. A lack of membrane dynamics outside the stimulated ROI in the ArchT cell suggests a localized membrane response in or near the stimulation ROI. This stimulation region response is unlikely to be driven by heat or light as control cells lack any similar membrane dynamics in the

stimulation region (Figure 3C, Figure S5). These data support the hypothesis that spatiotemporal increases in pHi are sufficient to drive localized membrane ruffling responses in single cells.

Increases in pHi produce localized and dynamic membrane ruffling events

To quantify localized pHi-dependent membrane ruffling responses, we developed a custom analysis within NIS Elements (see methods). Briefly, each cell was segmented into a series of 2 μm wide concentric circles, originating from the circular stimulation region (Figure 4A). This segmentation allowed us to monitor membrane ruffling (change in cell area) as a function of distance from stimulation region. We observed that for ArchT stimulated cells, there was a distinct distance correlation (Figure 4B, additional representative cells in Figure S5), with the stimulation region (0 μm, red trace) and immediate neighbor regions (2–4 μm, pink traces) having a larger net change in area compared to more distant regions (6–20 μm, grey traces). Notably, all control cell data are less dynamic (smaller area change) compared to ArchT cells and there is no observed distance-dependence (Figure 4B, Figure S5).

In our initial analyses of membrane dynamics, we noted that some cells had pronounced localized protrusions with spatiotemporal increases in pHi while other cells exhibited both protrusion and retraction events in response to increased pHi. As these events would be lost in our previous analyses of net area change, we sought to quantify the *dynamics* of membrane responses in ArchT versus control. We modified the standard stimulation protocol to include a 30 sec observation period before and after the stimulation period (see methods), allowing us to better compare membrane ruffling during stimulation to basal dynamics within the same cell.

To investigate these dynamics more closely, we quantified area change within the stimulation ROI for each cell. From this quantification, we identified 4 response phenotypes: increasing protrusive responses, dynamic responses, decreasing retraction responses, and static responses. As previously described, a subset of ArchT cells (25%) exhibited a strong protrusive response (increase in area) specifically during the photo-stimulation period (Figure 5A, left). A small number of control cells also exhibited smaller and light-independent protrusive responses, potentially indicating naturally occurring membrane protrusion events (Figure 5A, right). Interestingly, a large proportion of ArchT cells (35%) exhibited large, dynamic area changes during the photo-stimulation period (Figure 5B). Again, a small number of control cells also exhibited dynamic responses but in all cases the magnitude of responses was attenuated compared to ArchT cells (Figure 5B). Finally, for cells with retraction responses during the stimulation period, the ArchT and control cells had similar responses (Figure 5C). Unlike the other ArchT responses described, we note that retraction responses appear to be independent of stimulation light, with measured retraction prior to the stimulation window as well as during stimulation. This may suggest that depolymerization of actin fibers during retraction events dominate pHi-dependent protrusion events. While a few control cells fell into the "static response" category, we did not observe any ArchT cells that exhibited static or minimal dynamics throughout the stimulation window (Figure 5D).

Across all the cellular phenotypes, we noted that ArchT cells appeared to exhibit increased membrane dynamics specifically within the stimulation ROI. To confirm this, we first quantified relative area change, from one time point to the next, within the stimulation ROI of stimulated ArchT and control cells. We observed that the ArchT cells had distinct increase in dynamic area changes specifically within the stimulation period (Figure 5E). Control cells had no

clear increase in membrane dynamics during the stimulation window (Figure 5E). One caveat to these results is that Archaerhodopsins have been shown to hyperpolarize the cell membrane,[22,23,33] and previous work has linked membrane potential changes, both depolarization and hyperpolarization, to cytoskeleton remodeling on the timescale of 5-30 minutes[34,35] However, the localized membrane protrusion dynamics we observed occur on a much shorter timescale (30 sec-2.5 minutes), suggesting measured pHi increases are the key driving force behind the increased membrane dynamics. Taken together, these data suggest that ArchT induces localized pHi increases which in turn induce localized and dynamic membrane ruffling. Furthermore, our data suggest that photoactivation-dependent ruffling dynamics in ArchT cells are induced specifically by increased pHi.

DISCUSSION

Current approaches to manipulate pHi lack spatiotemporal control, limiting our understanding of the role of pHi dynamics in driving cellular processes. Furthermore, reliance on population-level analyses can also obscure a role for pHi in behavioral or phenotypic cellular heterogeneity. In this work, we have shown that the light-activated proton pump ArchT can be used as a robust optogenetic tool to spatiotemporally increase pHi in single-cells. The tool can be used to robustly increase pHi over the course of short time periods (minutes) and can be repeatedly stimulated to increase pHi for a longer period of time (~45 minutes). Using this tool, we show that spatially-restricted activation of ArchT can locally increase pHi and drive localized pHi-dependent membrane ruffling. Future work will investigate the dynamics membrane ruffling observed within ArchT cells with the goal of determining the molecular determinants of these

responses. Our current protocols should allow us to apply ArchT to investigate roles for pHi in regulating more complex single-cell behaviors such as cell polarization and migration.

The work described herein provides an experimental platform to transform our understanding of how pHi dynamics regulate normal cell behaviors. However, dysregulated pHi dynamics are a hallmark of diseases such as cancer (constitutively increased pHi)[6,7,12] and is thought to be an early event in cancer development.[8,36] Using ArchT to spatiotemporally increase pHi in single cells could allow us to probe whether increased pHi is a sufficient driver of single cell behaviors or whether increasing pHi in a single cell in an epithelial layer results in pHi communication to neighboring cells. With the development of the ArchT pHi manipulation protocols, these complex but critical questions of basic and cancer cell biology are now within our experimental grasp.

Conflicts of Interest Authors have no conflicts of interest to declare

Acknowledgments We would like to thank Dr. Yu-chen Hwang and Nikon Instruments Inc. Software Support Group for assistance developing the custom NIS Elements analysis pipeline. We would also like to thank members of the White lab for their helpful feedback on the manuscript.

Funding This work was supported by a DP2 (1DP2CA260416-01) to K.A.W.; C.E.T.D was supported by the Henry Luce Foundation and an O'Brien Family Summer Graduate Fellowship from the Institute of Precision Health at the University of Notre Dame, M.D.S. was supported by the University of Notre Dame STEM Scholars Program.

List of Supplemental Material

Supplemental Figures 1-5

Supplemental Videos 1-2

Video S1: Representative ArchT expressing cell with a stimulation region of interest (ROI) indicated as a red circle. The lamella of the cell is stimulated using the photoactivation protocol described in the methods using 561 nm light. A localized membrane ruffling response is observed within and directly adjacent to the stimulation ROI, quantified in Figure 4.

Video S2: Representative Control cell with a stimulation region of interest (ROI) indicated as a red circle. The lamella of the cell is stimulated using the photoactivation protocol described in the methods using 561 nm light. No localized membrane responses are observed, quantified in Figure 4.

FIGURES

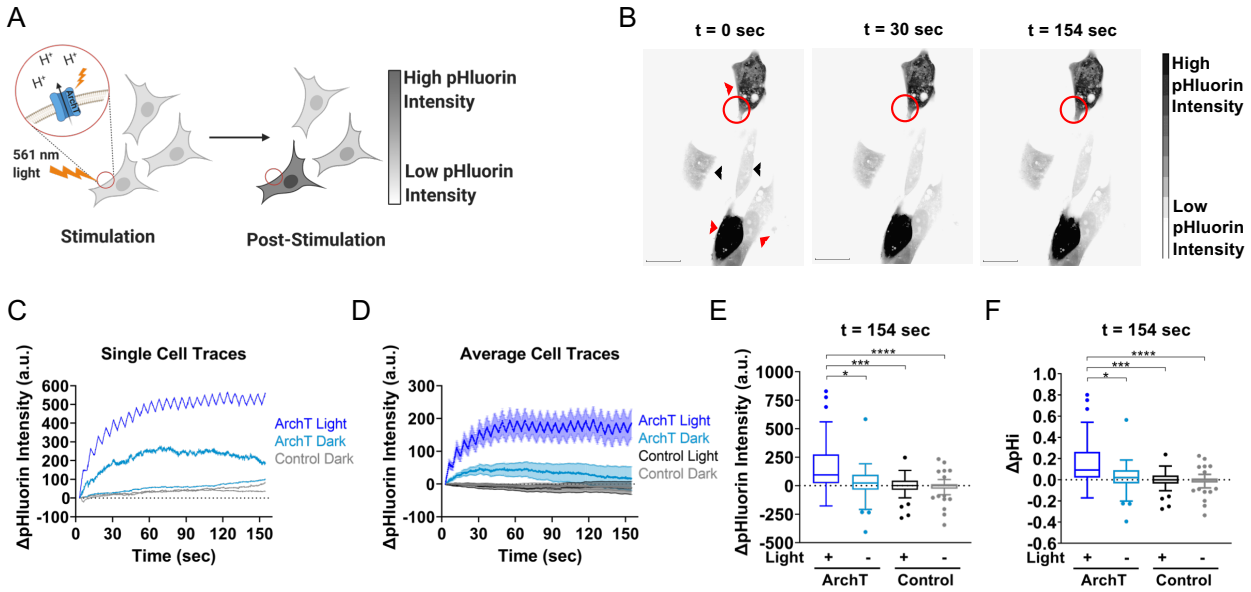

Figure 1. Archaerhodopsin can spatiotemporally increase pHi in single cells. (A) Experiment schematic showing RPE cells expressing Archaerhodopsin (ArchT) and a pH biosensor (pHluorin). Spatially-restricted activation of ArchT by 561 nm light can raise pHi in a single cell. **(B)** Representative field of view with ArchT-expressing cells (red arrowheads) and control cells without ArchT (black arrowheads). A single ArchT cell is photoactivated using a stimulation region of interest (ROI, red circle). Scale bar 20 µm. **(C)** Single-cell pHluorin intensity traces of cells from B. **(D)** Average of cell data collected as in B. Traces show mean ± SEM, from 3-5 biological replicates, n = 26-62 per condition. **(E)** Quantification of pHluorin intensity changes at the end of the experiment (t = 154 sec) for stimulated (+ Light) and unstimulated (- Light) ArchT and Control cells. **(F)** Change in pH intensity quantified for cells in E. For E and F, Tukey boxplots shown with significance determined using the Kruskal-Wallis test, Dunn's multiple comparison correction, * $p<0.05$, ***$p<0.001$, **** $p<0.0001$.

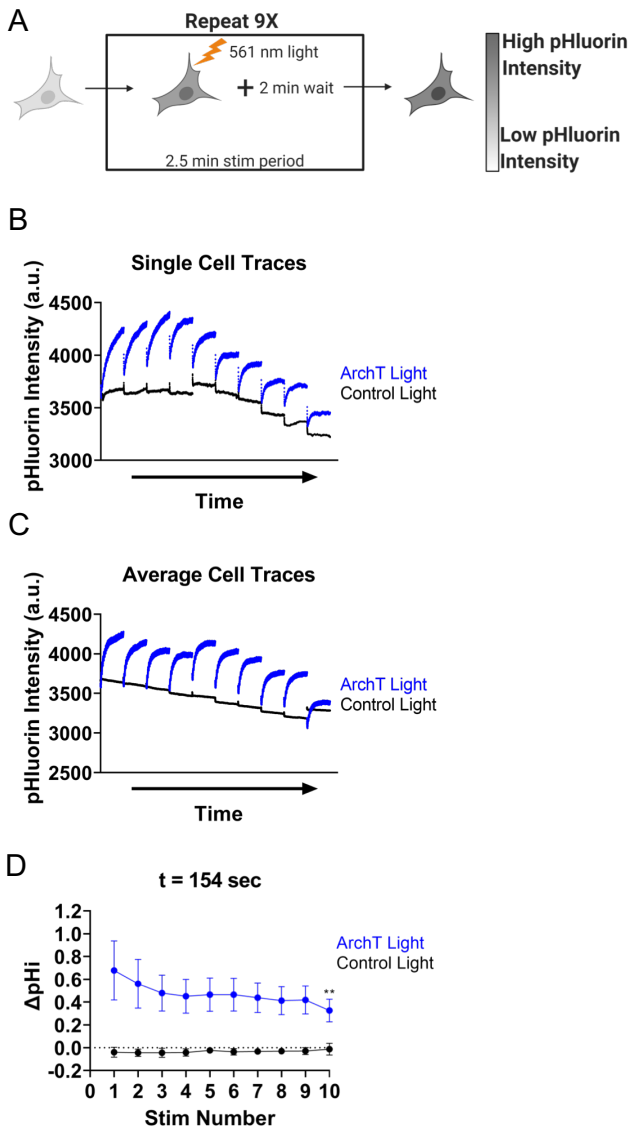

Figure 2. ArchT can be activated to repeatedly and robustly raise pHi in single cells. (A) Schematic of experimental design. Individual RPE cells expressing ArchT and pH biosensor (pHluorin) were stimulated using the standard protocol (see methods) followed by 2 minutes recovery. This pattern is repeated 9 times. (B) Single-cell pHluorin intensity traces of single ArchT (blue) and Control (black) cells treated as described in A. (C) Average cell data collected as in B. Traces show mean; 3-4 biological replicates across conditions, n = 9-10 per condition. (D) Change in pH intensity quantified for cells in C, mean ± SEM. For D, significance compared to Stim 1 determined using the two-way ANOVA, with Holm-Sidak multiple comparison correction, ** $p<0.01$.

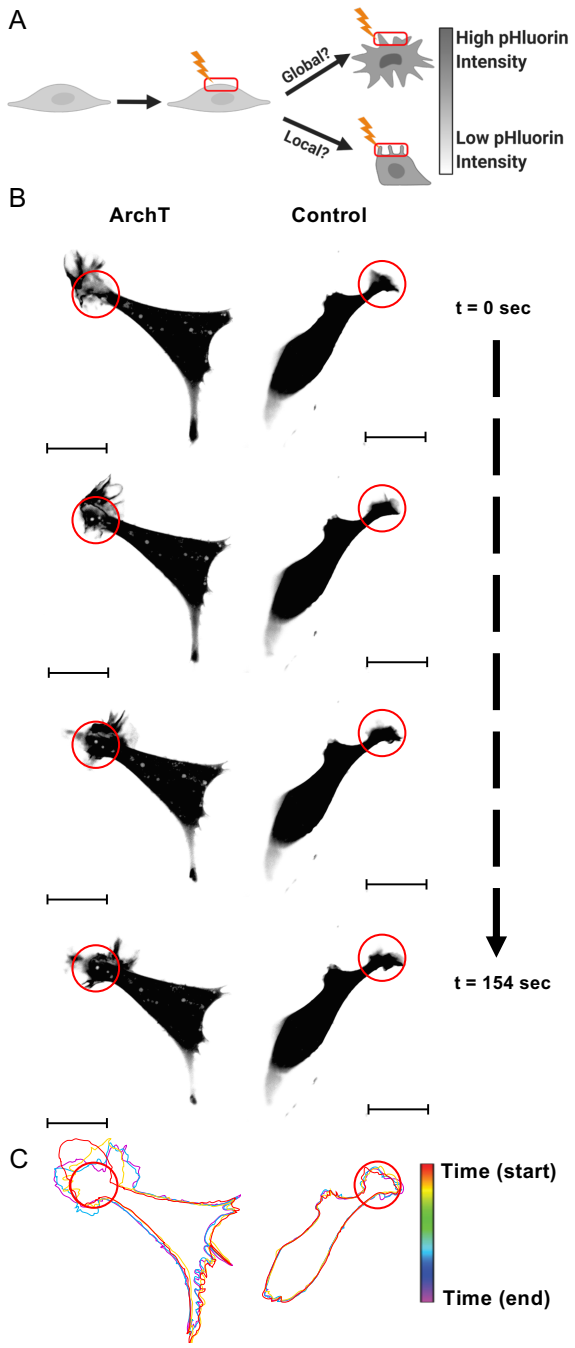

Figure 3. Increased pHi is a sufficient driver of local membrane protrusion events. (A) Schematic of experimental design. The lamella of the ArchT-expressing cell is stimulated with 561 nm light and cells are monitored for both global and local membrane ruffling events. (B) Representative images of ArchT and Control NIH3T3 cells treated as in A; stills from Supplementary Movies 1-2. Scale bar 20 µm. (C) For cells in B, membranes were traced at key movie frames and overlaid: t = 0 sec (red) to 154 sec (violet). Additional representative cells can be found in Figure S5.

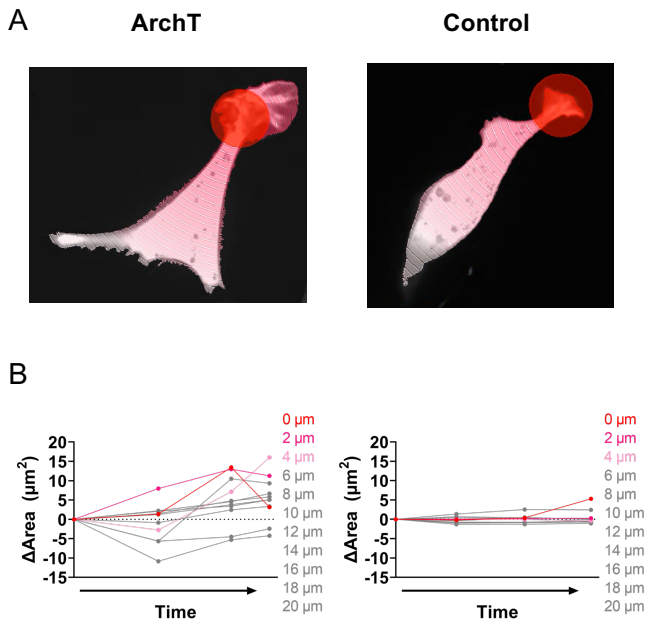

Figure 4. Quantification of local membrane protrusion events. (A) Representative segmentation analysis of cells in Figure 3 (see methods). Briefly, concentric segmentation circles radiate out at 2 μm intervals from the edge of the stimulation ROI (red circle). (B) Change in area for segmented ArchT (left) and Control (right) cells; where 0 μm indicates the stimulation ROI with increasing 2 μm intervals for each subsequent segment. Analysis of additional representative cells can be found in Figure S5.

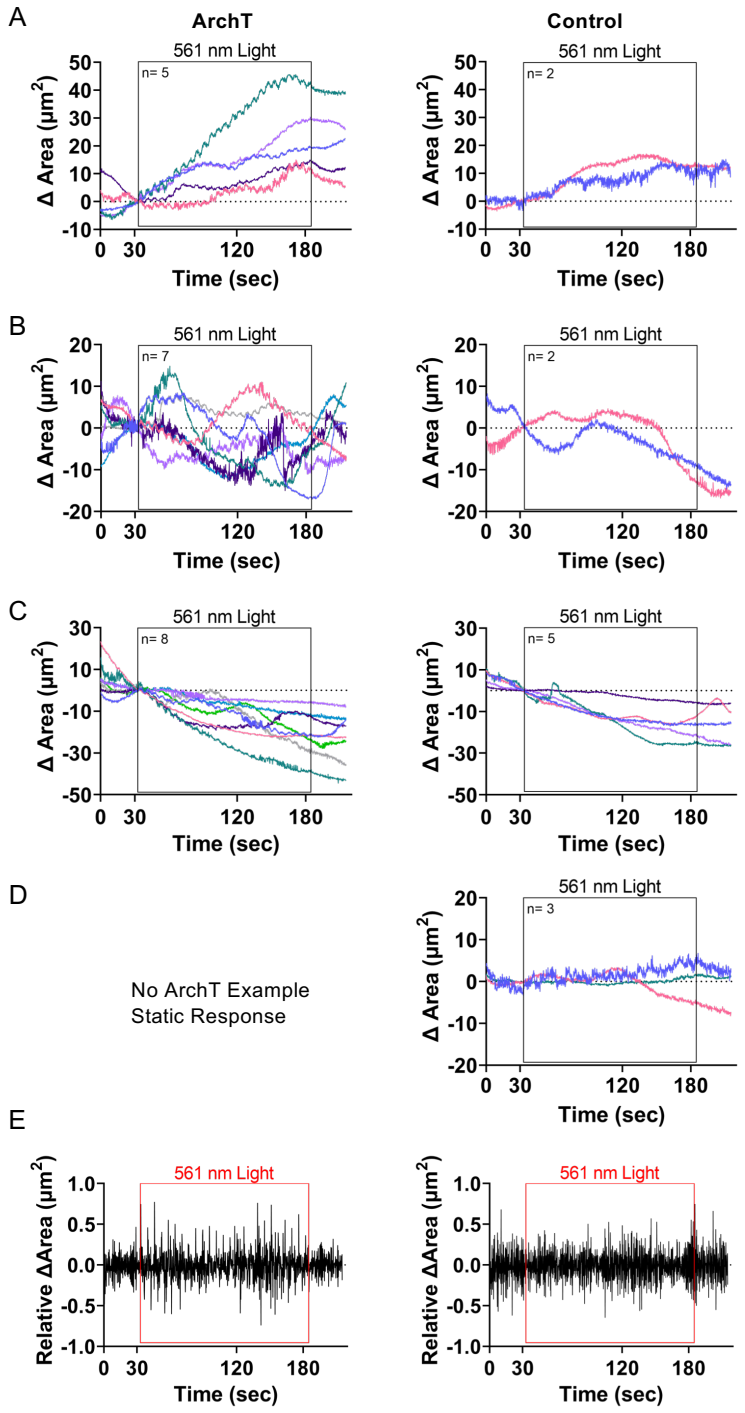

Figure 5. Increased pHi with ArchT induces increased membrane dynamics. (A-D) Single-cell area changes within the stimulation ROI for ArchT (left) and control (right) cells with increasing protrusive response phenotype (A), dynamic phenotype (B), decreasing retraction phenotype (C), and static phenotype (D). (E) Relative area changes for ArchT (left) and control (right) cells. From 3 biological replicates, n reported in figure panels.

Figure S1:

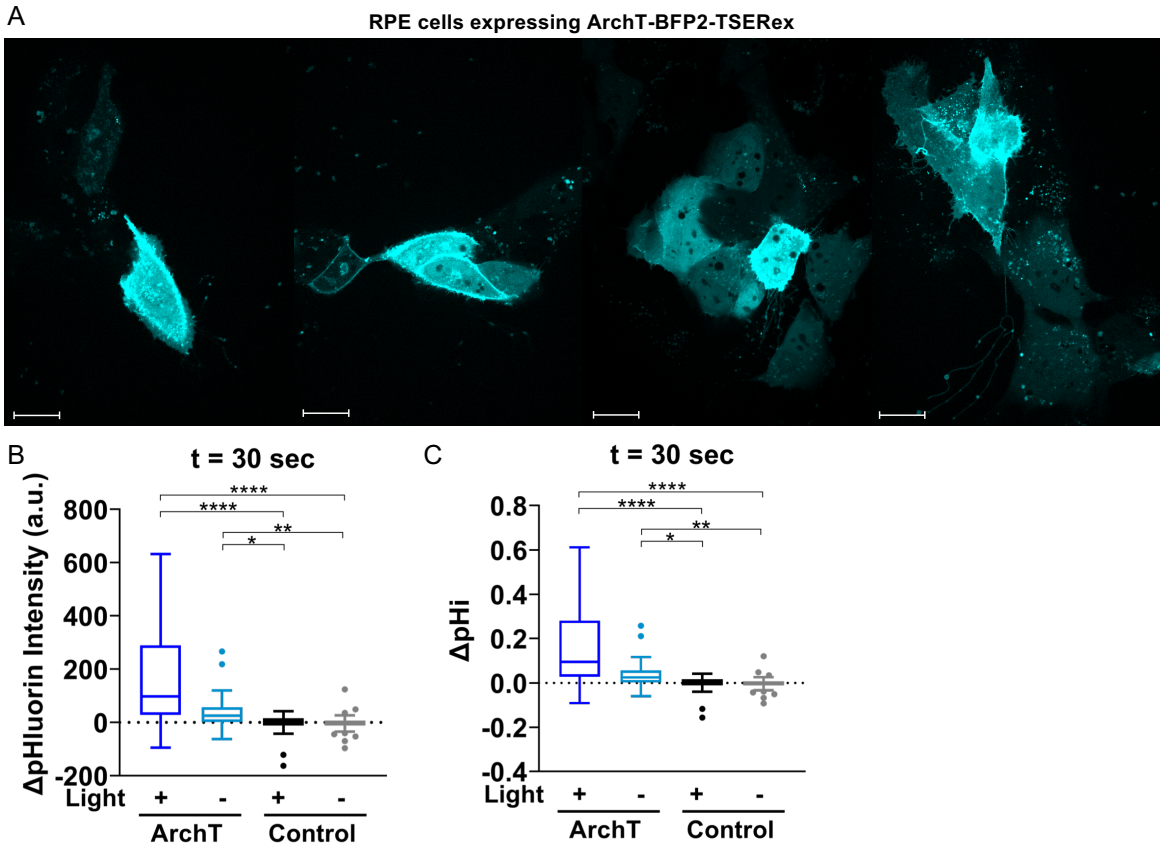

Figure S1: Archaerhodopsin Expression and Quantification of pHi increases in RPE cells (A) Representative images of RPE cells, expressing ArchT-BFP2-TSERex. Scale bar 20 µm (B) Quantification of pHluorin intensity changes at 30 seconds into experiment (30% LED power, Figure 1). Tukey boxplots of 3-5 biological replicates, n= 26-62 (C) Quantification of intracellular pH (pHi) at 30 seconds into experiment (30% LED power, Figure 1), based on intensity data in B. Tukey boxplots of 3-5 biological replicates, n= 26-62 (B-C) Significance determined using the Kruskal-Wallis test, Dunn's multiple comparison correction, *$p<0.05$, **$p<0.01$, and ****$p<0.0001$

Figure S2:

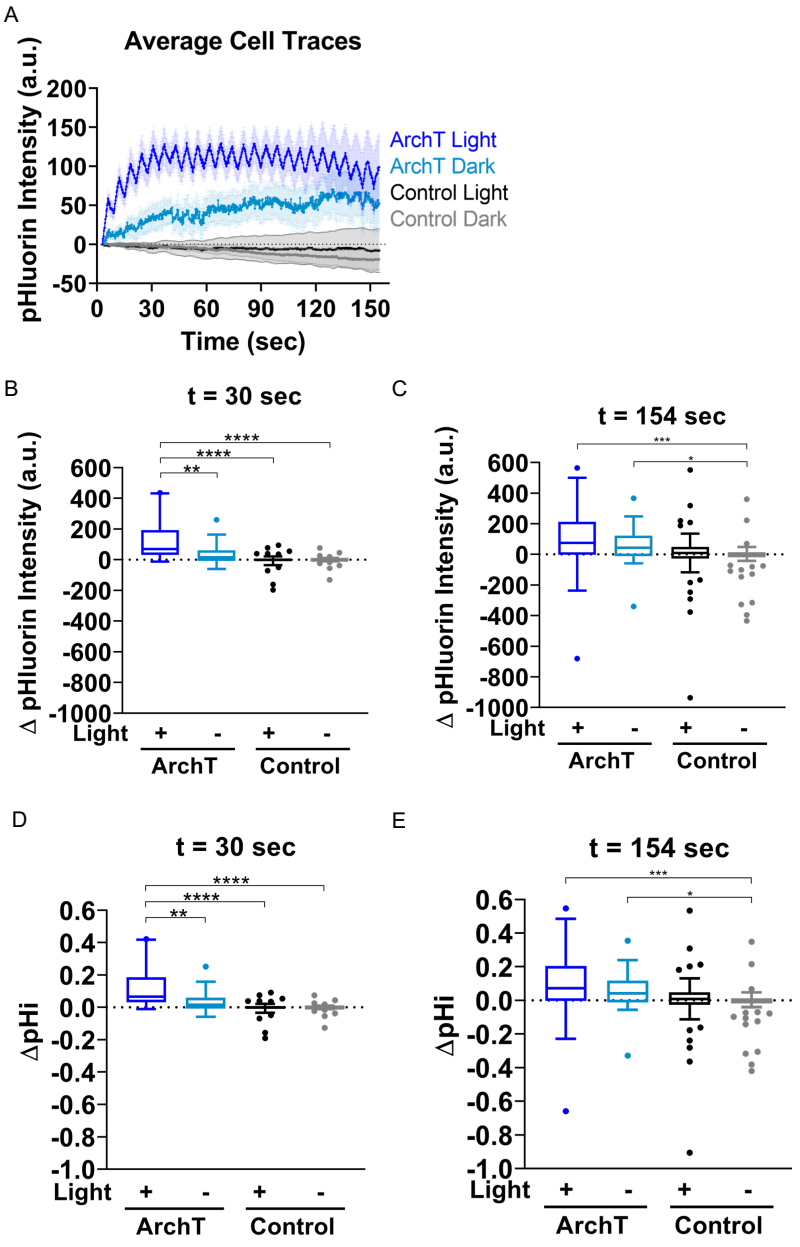

Figure S2: Archaerhodopsin can spatiotemporally increase pHi in single RPE cells using 100% LED Power. (A) Average pHluorin intensity traces over the course of the stimulation experiment. Traces show mean ± SEM. 3-5 biological replicates, n = 20-69 per condition. (B) Quantification of pHluorin intensity changes at 30 sec (B) and the end (C) of the experiment (t=154 sec) for stimulated (+Light) and unstimulated (-Light) ArchT and control cells. Change in pHi quantified for cells at 30 sec (D) and at the end of the experiment (E). For B-E, Tukey boxplots shown with significance determined using the Kruskal-Wallis test, Dunn's multiple comparison correction, *p<0.05, **p<0.01, ***p<0.001, and ****p<0.0001

Figure S3:

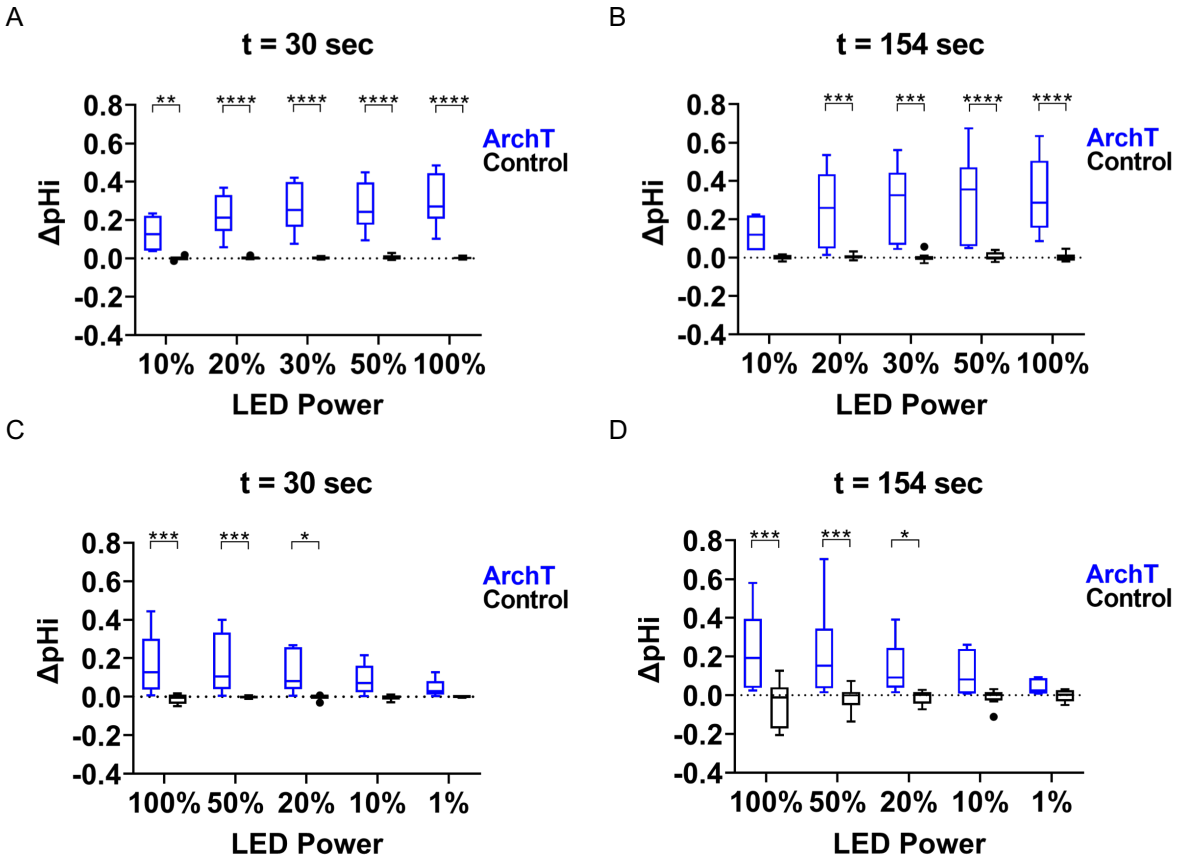

Figure S3: ArchT responses at a range of LED stimulation powers. Quantification of pHi change using an increasing sequence (10%, 20%, 30%, 50%, 100%) of LED stimulation power titration up at (A) 30 seconds and (B) at the end of the experiment (154 seconds). Quantification of pHi using a decreasing LED stimulation power sequence (100%, 50%, 20%, 10%, 1%) at (C) 30 seconds and (D) at the end of the experiment (154 seconds). (A-D) *$p<0.05$, **$p<0.01$, ***$p<0.001$, and ****$p<0.0001$. For A-D, Tukey boxplots shown, with Significance for A-D determined using two-way ANOVA and Holm-Šídák's multiple comparison test, and sphericity was assumed for these analyses. 1-3 biological replicates, n= 6-8 per condition.

Figure S4:

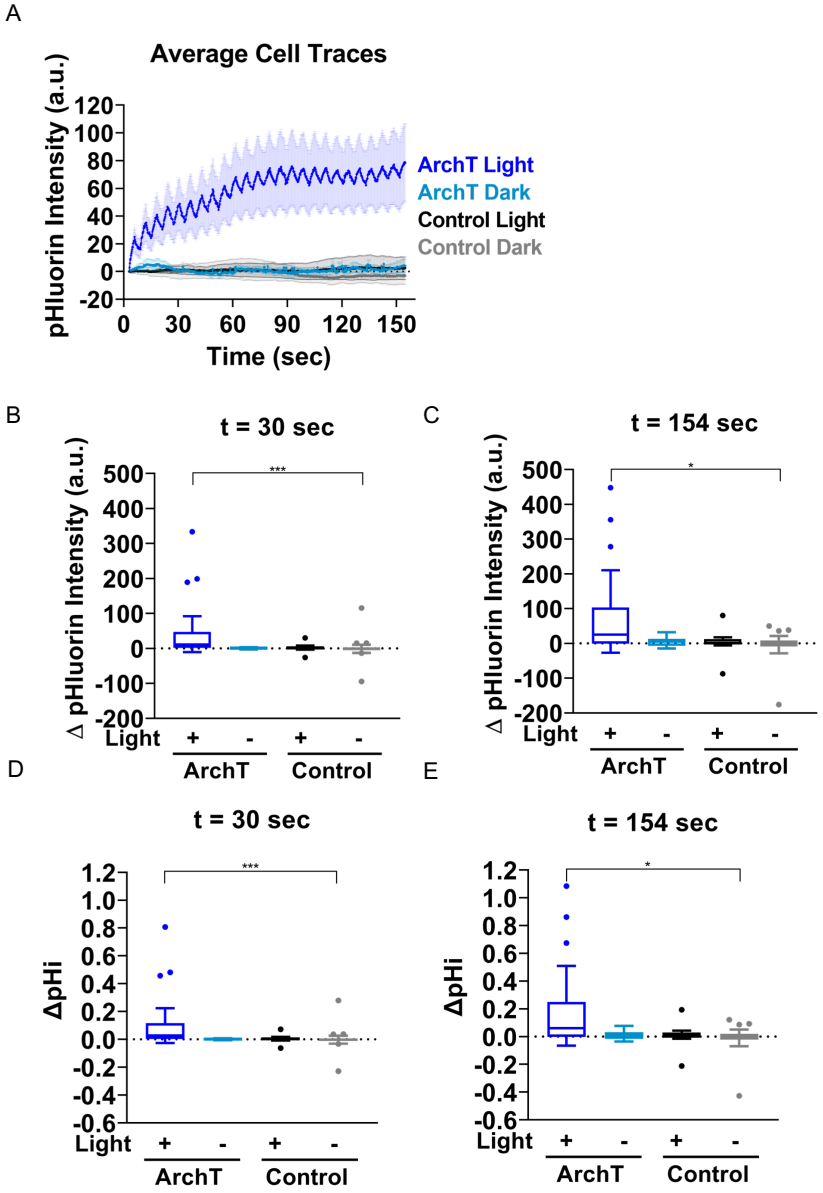

Figure S4: Archaerhodopsin can spatiotemporally increase pHi in single NIH-3T3 cells. (A) Average pHluorin intensity traces over the course of the stimulation experiment. Traces show mean ± SEM. 3 biological replicates, n = 9-31 per condition. (B) Quantification of pHluorin intensity changes at 30 sec (B) and the end (C) of the experiment (t=154 sec) for stimulated (+Light) and unstimulated (-Light) ArchT and control cells. Change in pHi quantified for cells at 30 sec (D) and at the end of the experiment (F). For B-E, Tukey boxplots shown with significance determined using the Kruskal-Wallis test, Dunn's multiple comparison correction, *p<0.05, **p<0.01, and ****p<0.0001.

Figure S5:

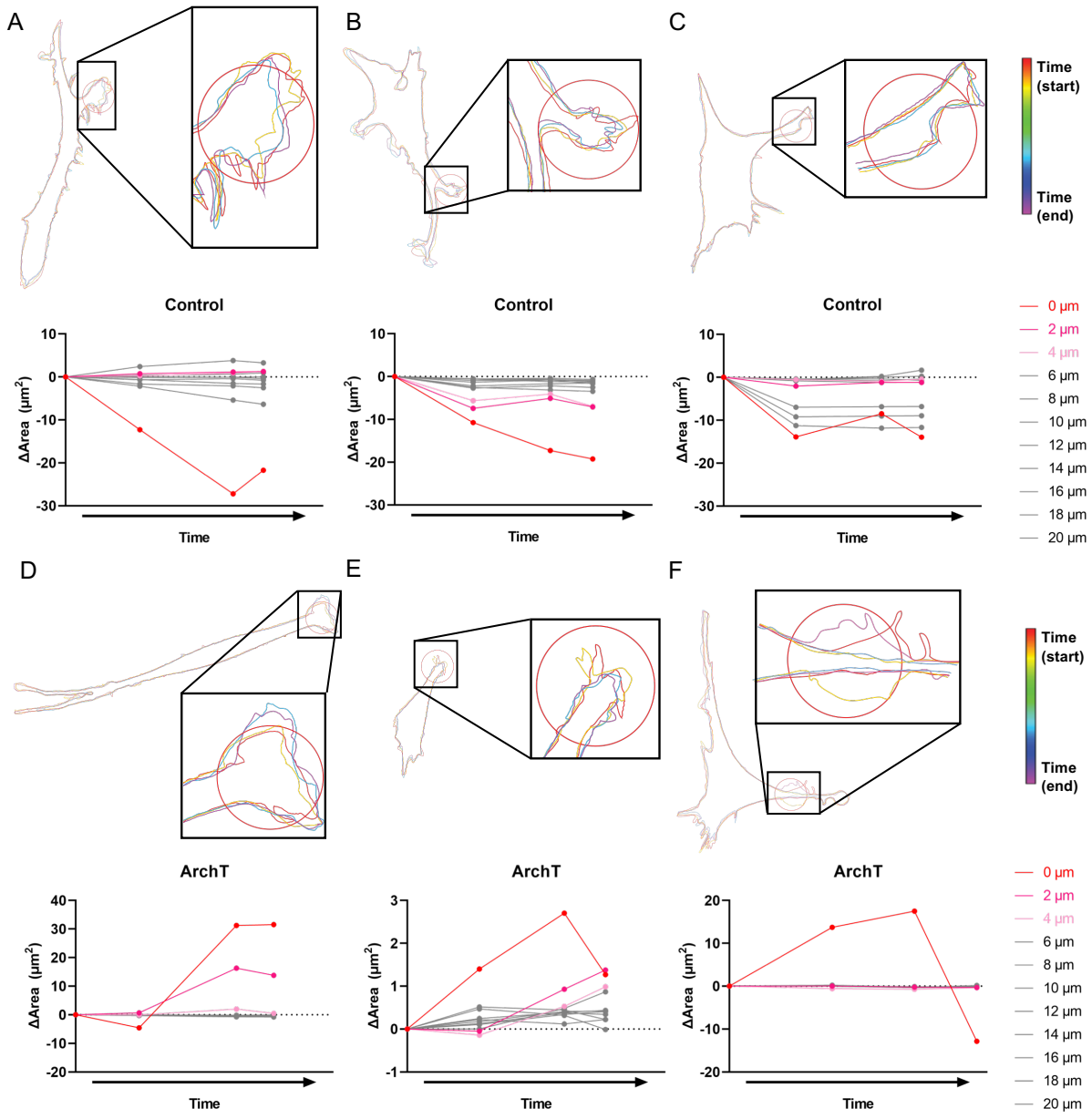

Figure S5. Additional Membrane Responses for NIH-3T3 cells treated as in Figure 3. Additional representative images of Control (A-C) and ArchT expressing (D-F) NIH-3T3 cells stimulated with 561 nm light. As in Figure 3, membranes were traced at key movie frames and overlayed, t= 0 sec (red) to 154 sec (violet). Zoomed-in sections of the stimulation region and the membrane dynamics are also provided. Change in area for segmented cells are located below their respective trace. 0 µm indicates the stimulation ROI with each subsequent segment representing 2µm intervals.

Bibliography:

(1) Frantz, C.; Karydis, A.; Nalbant, P.; Hahn, K. M.; Barber, D. L. Positive Feedback between Cdc42 Activity and H^+ Efflux by the Na-H Exchanger NHE1 for Polarity of Migrating Cells. *The Journal of Cell Biology* **2007**, *179* (3), 403–410. https://doi.org/10.1083/jcb.200704169.

(2) Denker, S. P.; Barber, D. L. Cell Migration Requires Both Ion Translocation and Cytoskeletal Anchoring by the Na-H Exchanger NHE1. *The Journal of Cell Biology* **2002**, *159* (6), 1087–1096. https://doi.org/10.1083/jcb.200208050.

(3) Frantz, C.; Barreiro, G.; Dominguez, L.; Chen, X.; Eddy, R.; Condeelis, J.; Kelly, M. J. S.; Jacobson, M. P.; Barber, D. L. Cofilin Is a PH Sensor for Actin Free Barbed End Formation: Role of Phosphoinositide Binding. *J. Cell Biol.* **2008**, *183* (5), 865–879. https://doi.org/10.1083/jcb.200804161.

(4) Srivastava, J.; Barreiro, G.; Groscurth, S.; Gingras, A. R.; Goult, B. T.; Critchley, D. R.; Kelly, M. J. S.; Jacobson, M. P.; Barber, D. L. Structural Model and Functional Significance of PH-Dependent Talin-Actin Binding for Focal Adhesion Remodeling. *Proceedings of the National Academy of Sciences* **2008**, *105* (38), 14436–14441. https://doi.org/10.1073/pnas.0805163105.

(5) Martin, C.; Pedersen, S. F.; Schwab, A.; Stock, C. Intracellular PH Gradients in Migrating Cells. *American Journal of Physiology-Cell Physiology* **2010**, *300* (3), C490–C495. https://doi.org/10.1152/ajpcell.00280.2010.

(6) Webb, B. A.; Chimenti, M.; Jacobson, M. P.; Barber, D. L. Dysregulated PH: A Perfect Storm for Cancer Progression. *Nat. Rev. Cancer* **2011**, *11* (9), 671–677. https://doi.org/10.1038/nrc3110.

(7) Czowski, B. J.; Romero-Moreno, R.; Trull, K. J.; White, K. A. Cancer and PH Dynamics: Transcriptional Regulation, Proteostasis, and the Need for New Molecular Tools. *Cancers (Basel)* **2020**, *12* (10). https://doi.org/10.3390/cancers12102760.

(8) Grillo-Hill, B. K.; Choi, C.; Jimenez-Vidal, M.; Barber, D. L. Increased H+ Efflux Is Sufficient to Induce Dysplasia and Necessary for Viability with Oncogene Expression. *eLife* **2015**, *4*, e03270. https://doi.org/10.7554/eLife.03270.

(9) Parks, S. K.; Cormerais, Y.; Durivault, J.; Pouyssegur, J. Genetic Disruption of the PHi-Regulating Proteins Na+/H+ Exchanger 1 (SLC9A1) and Carbonic Anhydrase 9 Severely Reduces Growth of Colon Cancer Cells. *Oncotarget* **2016**, *8* (6), 10225–10237. https://doi.org/10.18632/oncotarget.14379.

(10) Slepkov, E. R.; Rainey, J. K.; Sykes, B. D.; Fliegel, L. Structural and Functional Analysis of the Na+/H+ Exchanger. *Biochem J* **2007**, *401* (Pt 3), 623–633. https://doi.org/10.1042/BJ20061062.

(11) Stock, C.; Schwab, A. Role of the Na/H Exchanger NHE1 in Cell Migration. *Acta Physiol (Oxf)* **2006**, *187* (1–2), 149–157. https://doi.org/10.1111/j.1748-1716.2006.01543.x.

(12) White, K. A.; Grillo-Hill, B. K.; Barber, D. L. Cancer Cell Behaviors Mediated by Dysregulated PH Dynamics at a Glance. *J. Cell. Sci.* **2017**, *130* (4), 663–669. https://doi.org/10.1242/jcs.195297.

(13) Olesen, C. W.; Vogensen, J.; Axholm, I.; Severin, M.; Schnipper, J.; Pedersen, I. S.; von Stemann, J. H.; Schrøder, J. M.; Christensen, D. P.; Pedersen, S. F. Trafficking, Localization and Degradation of the Na + ,HCO 3 − Co-Transporter NBCn1 in Kidney and Breast Epithelial Cells. *Scientific Reports* **2018**, *8* (1), 7435. https://doi.org/10.1038/s41598-018-25059-7.

(14) Rolver, M. G.; Elingaard-Larsen, L. O.; Andersen, A. P.; Counillon, L.; Pedersen, S. F. Pyrazine Ring-Based Na+/H+ Exchanger (NHE) Inhibitors Potently Inhibit Cancer Cell Growth in 3D Culture, Independent of NHE1. *Sci Rep* **2020**, *10*. https://doi.org/10.1038/s41598-020-62430-z.

(15) Mauvezin, C.; Nagy, P.; Juhász, G.; Neufeld, T. P. Autophagosome–Lysosome Fusion Is Independent of V-ATPase-Mediated Acidification. *Nature Communications* **2015**, *6* (1), 7007. https://doi.org/10.1038/ncomms8007.

(16) Yuan, Y.; Shimura, M.; Hughes, B. A. Regulation of Inwardly Rectifying K+ Channels in Retinal Pigment Epithelial Cells by Intracellular PH. *The Journal of Physiology* **2003**, *549* (2), 429–438. https://doi.org/10.1113/jphysiol.2003.042341.

(17) Grinstein, S.; Romanek, R.; Rotstein, O. D. Method for Manipulation of Cytosolic PH in Cells Clamped in the Whole Cell or Perforated-Patch Configurations. *Am J Physiol* **1994**, *267* (4 Pt 1), C1152-1159. https://doi.org/10.1152/ajpcell.1994.267.4.C1152.

(18) Ellis-Davies, G. C. R. Caged Compounds: Photorelease Technology for Control of Cellular Chemistry and Physiology. *Nat Methods* **2007**, *4* (8), 619–628. https://doi.org/10.1038/nmeth1072.

(19) Kim, J. H.; Demaurex, N.; Grinstein, S. Chapter 20 Intracellular PH: Measurement, Manipulation and Physiological Regulation. In *Handbook of Biological Physics*; Konings, W. N., Kaback, H. R., Lolkema, J. S., Eds.; Transport Processes in Eukaryotic and Prokaryotic Organisms; North-Holland, 1996; Vol. 2, pp 447–472. https://doi.org/10.1016/S1383-8121(96)80061-3.

(20) Hulikova, A.; Swietach, P. Nuclear Proton Dynamics and Interactions with Calcium Signaling. *Journal of Molecular and Cellular Cardiology* **2016**, *96*, 26–37. https://doi.org/10.1016/j.yjmcc.2015.07.003.

(21) Miesenböck, G. Optogenetic Control of Cells and Circuits. *Annu Rev Cell Dev Biol* **2011**, *27*, 731–758. https://doi.org/10.1146/annurev-cellbio-100109-104051.

(22) Chow, B. Y.; Han, X.; Dobry, A. S.; Qian, X.; Chuong, A. S.; Li, M.; Henninger, M. A.; Belfort, G. M.; Lin, Y.; Monahan, P. E.; Boyden, E. S. High-Performance Genetically Targetable Optical Neural Silencing by Light-Driven Proton Pumps. *Nature* **2010**, *463* (7277), 98–102. https://doi.org/10.1038/nature08652.

(23) Han, X.; Chow, B. Y.; Zhou, H.; Klapoetke, N. C.; Chuong, A.; Rajimehr, R.; Yang, A.; Baratta, M. V.; Winkle, J.; Desimone, R.; Boyden, E. S. A High-Light Sensitivity Optical Neural Silencer: Development and Application to Optogenetic Control of Non-Human Primate Cortex. *Front. Syst. Neurosci.* **2011**, *5*. https://doi.org/10.3389/fnsys.2011.00018.

(24) El-Gaby, M.; Zhang, Y.; Wolf, K.; Schwiening, C. J.; Paulsen, O.; Shipton, O. A. Archaerhodopsin Selectively and Reversibly Silences Synaptic Transmission through Altered PH. *Cell Rep* **2016**, *16* (8), 2259–2268. https://doi.org/10.1016/j.celrep.2016.07.057.

(25) Wu, L.; Dong, A.; Dong, L.; Wang, S.-Q.; Li, Y. PARIS, an Optogenetic Method for Functionally Mapping Gap Junctions. *eLife 8*. https://doi.org/10.7554/eLife.43366.

(26) Choi, C.-H.; Webb, B. A.; Chimenti, M. S.; Jacobson, M. P.; Barber, D. L. PH Sensing by FAK-His58 Regulates Focal Adhesion Remodeling. *The Journal of Cell Biology* **2013**, *202* (6), 849–859. https://doi.org/10.1083/jcb.201302131.

(27) Koivusalo, M.; Welch, C.; Hayashi, H.; Scott, C. C.; Kim, M.; Alexander, T.; Touret, N.; Hahn, K. M.; Grinstein, S. Amiloride Inhibits Macropinocytosis by Lowering Submembranous PH and Preventing Rac1 and Cdc42 Signaling. *Journal of Cell Biology* **2010**, *188* (4), 547–563. https://doi.org/10.1083/jcb.200908086.

(28) Flinck, M.; Kramer, S. H.; Pedersen, S. F. Roles of PH in Control of Cell Proliferation. *Acta Physiologica* **2018**, *223* (3), e13068. https://doi.org/10.1111/apha.13068.

(29) Rappel, W.-J.; Edelstein-Keshet, L. Mechanisms of Cell Polarization. *Curr Opin Syst Biol* **2017**, *3*, 43–53. https://doi.org/10.1016/j.coisb.2017.03.005.

(30) Gov, N. S.; Gopinathan, A. Dynamics of Membranes Driven by Actin Polymerization. *Biophys J* **2006**, *90* (2), 454–469. https://doi.org/10.1529/biophysj.105.062224.

(31) *Propagation of Protons at the Water Membrane Interface Microscopic Evaluation of a Macroscopic Process*; CRC Press, 2017; pp 259–276. https://doi.org/10.1201/9780203743805-12.

(32) Wu, Y. I.; Frey, D.; Lungu, O. I.; Jaehrig, A.; Schlichting, I.; Kuhlman, B.; Hahn, K. M. A Genetically-Encoded Photoactivatable Rac Controls the Motility of Living Cells. *Nature* **2009**, *461* (7260), 104–108. https://doi.org/10.1038/nature08241.

(33) Adams, D. S.; Tseng, A.-S.; Levin, M. Light-Activation of the Archaerhodopsin H+-Pump Reverses Age-Dependent Loss of Vertebrate Regeneration: Sparking System-Level Controls in Vivo. *Biology Open* **2013**, *2* (3), 306–313. https://doi.org/10.1242/bio.20133665.

(34) Nin, V.; Hernández, J. A.; Chifflet, S. Hyperpolarization of the Plasma Membrane Potential Provokes Reorganization of the Actin Cytoskeleton and Increases the Stability of

Adherens Junctions in Bovine Corneal Endothelial Cells in Culture. *Cell Motility* **2009**, *66* (12), 1087–1099. https://doi.org/10.1002/cm.20416.

(35) Chifflet, S.; Hernández, J. A.; Grasso, S.; Cirillo, A. Nonspecific Depolarization of the Plasma Membrane Potential Induces Cytoskeletal Modifications of Bovine Corneal Endothelial Cells in Culture. *Experimental Cell Research* **2003**, *282* (1), 1–13. https://doi.org/10.1006/excr.2002.5664.

(36) Sharma, M.; Astekar, M.; Soi, S.; Manjunatha, B. S.; Shetty, D. C.; Radhakrishnan, R. PH Gradient Reversal: An Emerging Hallmark of Cancers. *Recent Pat Anticancer Drug Discov* **2015**, *10* (3), 244–258. https://doi.org/10.2174/1574892810666150708110608.